Luminescence properties and scintillation mechanisms of cerium- and praseodymium-doped lutetium orthoaluminate



1997 J. Phys.: Condens. Matter 9 5229

(http://iopscience.iop.org/0953-8984/9/24/019)

J. Phys.: Condens. Matter **9** (1997) 5229–5243. Printed in the UK PII: S0953-8984(97)80644-3

# Luminescence properties and scintillation mechanisms of cerium- and praseodymium-doped lutetium orthoaluminate

C Dujardin†, C Pedrini†, J C Gâcon†, A G Petrosyan‡, A N Belsky§ and A N Vasil'ev§

† Laboratoire de Physico-Chimie des Matériaux Luminescents, Université Claude Bernard, Lyon I, Unité Mixte de Recherche 5620 CNRS, 43, Boulevard du 11 Novembre 1918, 69622 Villeurbanne Cédex, France

‡ Institute for Physical Research, Armenian Academy of Science, 378410 Ashtarak-2, Armenia

§ Synchrotron Radiation Laboratory, Faculty of Physics, Moscow State University, 119899 Moscow, Russia

Received 3 January 1997

**Abstract.** Absorption, reflection as well as luminescence emission, excitation, and decay curves for single crystals of $LuAlO_3:Ce^{3+}$ and $LuAlO_3:Pr^{3+}$ grown by the Bridgman technique have been measured at various temperatures. The fluorescence spectra photo-excited over a wide energy domain ranging from the UV to the x-ray region, and the kinetics are typical of the cerium and praseodymium ions. These experimental results show that the exciton transfer to the dopant occurs at around 8 eV, and the energy transfer via sequential hole and electron trapping is dominant at higher energy. This process must be considered as the main scintillation mechanism in this crystal. The high efficiency of this mechanism is explained by the small energy difference between the 4f level of the dopant and the top of the valence band, estimated from XPS measurements.

## 1. Introduction

Research into and development of inorganic scintillators is very active nowadays, because radiation detectors are used in many devices, and there is a strong demand for improving performances. Since scintillation detectors are found in many and various fields, scintillator requirements are correspondingly different [1]. For many applications, like medical diagnostics, using x-ray computing tomography or positron emission tomography, high light yield, fast scintillation, and high stopping power are the most important requirements.

The development of new scintillator crystals needs a good understanding of the scintillation mechanisms. When a high-energy photon is absorbed, a large number of secondary excitations are generated. The energy relaxation and interactions between these excitations lead to low-energy photons: the luminescence. The main processes involved in the scintillation mechanisms are: (i) multiplication of excitations (Auger relaxation of holes and inelastic scattering of electrons); (ii) thermalization of the excitation and migration; (iii) autolocalization and excitation transfer to the states in the forbidden band; and (iv) radiative and non-radiative recombination.

Each process occurs in its own energy and time ranges. Synchrotron radiation (SR) exhibits a continuum spectrum from the UV to the x-ray region, with light pulses with time resolution below 1 ns. Time-resolved spectroscopy using SR is a very efficient method for the analysis of scintillation processes [2].

0953-8984/97/245229+15$19.50  

Orthoaluminate crystals with a perovskite-like structure and doped with $Ce^{3+}$ or $Pr^{3+}$ ions have been investigated for scintillator applications—in particular, $YAlO_3$ [3–5]—and a high light output has been measured (26 000 photons $MeV^{-1}$ for $YAlO_3:Ce^{3+}$ crystal). However, $YAlO_3$ material has a low density (5.35 g $cm^{-3}$). On the other hand, lutetium compounds doped with $Ce^{3+}$ ions seem to have attractive scintillation properties. Examples are orthosilicate [6] $Lu_2SiO_5:Ce^{3+}$ and orthophosphate [7] $LuPO_4:Ce^{3+}$. The substitution of Lu for Y in $YAlO_3$ increases the density to 8.34 g $cm^{-3}$. Nevertheless, the $^{176}Lu$ isotope is radioactive (1 MeV/$\beta$), but gives rise to a small background count of 200 $s^{-1}$ [8]. $LuAlO_3:Ce^{3+}$ is nowadays very actively investigated, but the scintillation mechanisms [9–13] are not yet well understood.

The purpose of this paper is to determine the luminescence properties of $LuAlO_3$ doped with $Ce^{3+}$ and $Pr^{3+}$ ions, and to propose a model which can describe the scintillation mechanism involved in these compounds.

## 2. Experimental details

### *2.1. Crystal growth*

Single crystals of the $LuAlO_3:Ce^{3+}$ and $LuAlO_3:Pr^{3+}$ orthoaluminates (space group $D_{16}^{2h}$—*Pbnm*) were grown using the Bridgman technique, details of which have been given in references [14] and [15]. High-purity oxides of lutetium, cerium, and praseodymium, and small-grain vacuum-melted crystalline sapphire (all of 3 to 4N specification) were used. The melts, of stoichiometric compositions, were prepared in Mo crucibles under argon/hydrogen atmosphere. The melting temperature has been recorded as 1900 °C ± 15 °C using the melting temperatures of $Y_3Al_5O_{12}$ (YAG) (1940 °C) and $Tb_3Al_5O_{12}$ (1865 °C) as calibration points. Growth rates of 1.5–2 mm $h^{-1}$ were used. The resulting crystals were optically transparent, single phase, and free of light scattering, as checked by x-ray diffraction and optical microscopy. The Ce content was measured for two samples (0.05 at.% and 0.47 at.%) using the spectra emission technique. The concentration of praseodymium in the Pr-doped crystals investigated was not measured; the Pr concentration in the melt was 0.6 at.%, and the real concentration is expected to be much less, due to the low distribution coefficient (0.17 for Ce in $LuAlO_3$) [15].

### *2.2. The experimental set-up*

Absorption measurements were made using a Cary UV–visible–NIR spectrophotometer, model 2300, at room temperature, and with a cryostat from SMC at low temperature. The samples used were made very thin (≈100 $\mu$m) owing to the strong absorption coefficient. In the region of the fundamental absorption above 7 eV, reflectivity spectra were recorded using the synchrotron radiation of the SuperACO storage ring of LURE in France. The reflectivity was measured in the direction making a 20° angle with the incident light beam. The reference beam was given by the excitation spectrum of sodium salicylate. Using Kramers–Krönig transformations, the absorption spectrum from 7 eV to 40 eV was calculated from the reflectivity measurements.

For excitation with energy from 4 eV to 100 eV, the light source used was the storage ring of SuperACO. It operates in a multiple-bunches mode (24 bunches per repetition period of 240 ns) for excitation spectra. The normal-incidence monochromator, with a 3 m toroidal holographic grating with 300 lines $mm^{-1}$ at the beam line SA61, allowed us to excite crystals in the range 4–40 eV, whereas the grazing-incidence monochromator, with a 2.2 m toroidal

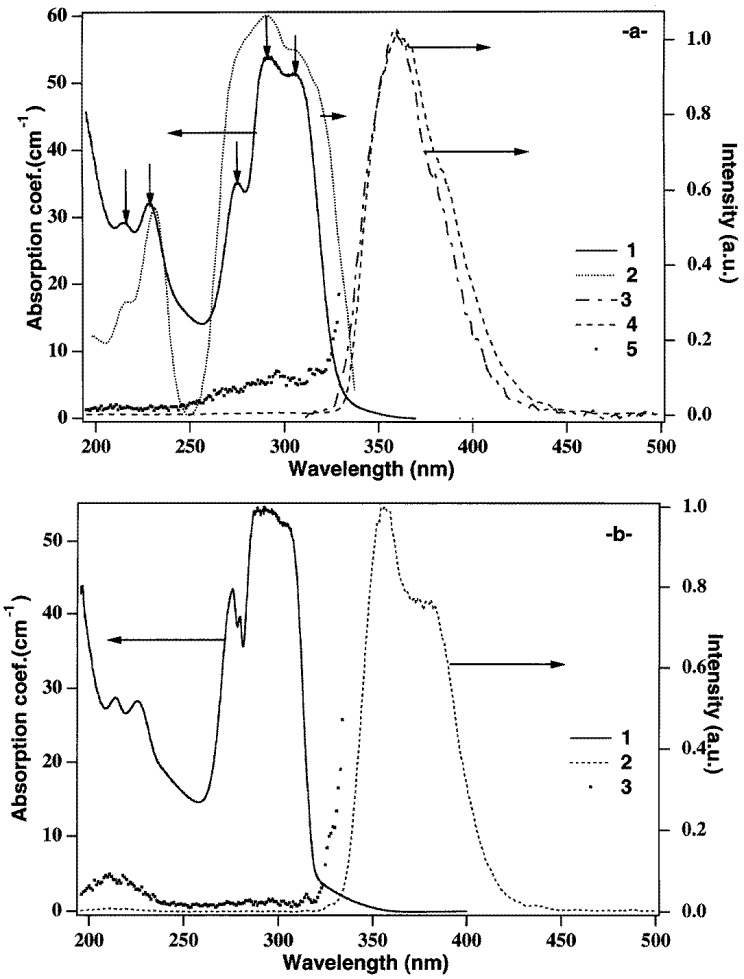


**Figure 1.** $LuAlO_3:Ce^{3+}$. (a) At room temperature. 1: the absorption spectrum; 2: the excitation spectrum ($\lambda_{em} = 360$ nm); 3: UV-induced emission ($\lambda_{exc} = 320$ nm); 4: x-ray-induced emission; and 5: the high-energy part of the x-ray-induced emission ($\times 15$). (b) 1: the absorption spectrum at $T \approx 10$ K; 2: the x-ray-induced emission at $T \approx 77$ K; and 3: the high-energy part of the x-ray induced emission ($\times 10$).

grating with 1800 lines mm$^{-1}$ at the beam line SA71, was used to excite crystals with photons in the range 22–100 eV. The fluorescence was detected with a photomultiplier: Hamamatsu 5321. Emission light was selected through interference filters. For decay measurements, SuperACO synchrotron radiation in the two-bunches mode was used. The width of the pulses was 0.6 ns, with a repetition rate of 120 ns. A time-to-pulse converter, and a multichannel analyser (150 ps/channel) were used for recording the decays.

Emission spectra obtained under UV excitation were taken at the laboratory in Lyon using Q-switched $Y_3Al_5O_{12}:Nd^{3+}$, the pumped-dye-laser beam being frequency doubled and mixed with the fundamental. The analysis and the detection of the fluorescence were performed with a computer-scannable 1 m Hilger monochromator and a Hamamatsu 9789 phototube.

Luminescence spectra and the decay kinetics under x-ray excitation have been measured using synchrotron radiation from the wiggler of the storage ring VEPP-3 (INP, Novosibirsk). SR x-ray exciting pulses of $10^6$ photons, with a repetition rate of 250 ns, cover the spectral range from 1 to 100 keV. For the luminescence measurement, a monochromator, MDR-23, and a dissector, LI-602 [16], with time resolution of 20 ps have been used. The FWHM of the SR pulses was 0.5 ns, leading to a time resolution of 100 ps.

## 3. Experimental results

### *3.1. UV absorption and emission spectra*

The optical properties of $LuAlO_3:Ce^{3+}$ are presented in figure 1. The electronic configuration of $Ce^{3+}$ is $4f^1$, giving rise to two spin–orbit levels, $^2F_{5/2}$ and $^2F_{7/2}$, separated by roughly 2000 $cm^{-1}$. In the UV range 200–400 nm, only f $\rightarrow$ d allowed electric dipole transitions are expected. The spatial extent of the wave function of the 5d electron is large, and the energy of the d states strongly depends on the crystal field. The absorption was examined in the near-ultra-violet region, from 200 to 400 nm, at liquid helium and room temperature. No resolved vibronic structure has been detected. In the spectral range between 200 and 320 nm, the spectra exhibit five main bands. The excitation spectrum (figure 1(a)) shows two groups of bands, one at low energy in the same range as the three absorption bands, and the other involving two bands between 200 and 250 nm. Finally, the five bands peaking at 216.4 nm and 231.7 nm for the first group, and at 275.6 nm, 292 nm, and 304 nm for the second group, can be assigned to the transitions from the ground state to the 5d level, which is completely split into five components as expected from the very low $C_s$ point symmetry of the Lu sites occupied by the $Ce^{3+}$ ions in $LuAlO_3$. The 5d levels of $Ce^{3+}$ in perovskite-like compounds are usually split into two groups (e and $t_2$) of levels [17]. An additional narrow peak is observed at around 274 nm at low temperature. Its width is much smaller, and it probably does not have the same origin as other bands. It can be connected with the $4f^7(^8S) \rightarrow 4f^7(^6I)$ transition of $Gd^{3+}$ impurities which has been observed at 279 nm for $LaF_3:Gd^{3+}$ [18]. These impurities also exhibit a very weak emission peak at 316 nm under x-ray excitation (figure 2(b)), which is assigned to the $4f^7(^8P) \rightarrow 4f^7(^6S)$ transition of $Gd^{3+}$.

The absorption coefficient at 250 nm is not zero, while no luminescence of $Ce^{3+}$ is detected under this excitation. The same phenomenon has been observed for $YAlO_3:Ce^{3+}$, and was explained by a broad absorption of $Ce^{4+}$ ions extending to 400 nm and overlapping the $Ce^{3+}$ emission [19]. As $Ce^{4+}$ has no 4f electron, this ion cannot absorb at this energy. But recent measurements show that the absorption coefficient at 250 nm depends upon the cerium concentration [20]. So the 250 nm absorption might be due to defects induced by $Ce^{4+}$, because the supplementary positive charge of this ion must be compensated by a structural defect for reasons of local electroneutrality. The 250 nm excitation gives rise to a 650 nm emission, but its assignment to defects associated with the presence of $Ce^{4+}$ is not clear, since this red emission is also observed for undoped $LuAlO_3$ crystal in which no $Ce^{3+}$ emission is detected [20].

Luminescence spectra have been obtained with different excitation sources (figure 1). Under x-ray synchrotron excitation, a strong broad emission was observed at around 375 nm, which is resolved into two components at liquid nitrogen temperature. The two peaks at 381 nm and 355 nm are separated by 1923 $cm^{-1}$, which represents the energy difference between the $^2F_{7/2}$ and $^2F_{5/2}$ spin–orbit levels of the $4f^1$ configuration of $Ce^{3+}$. Under 290 nm laser excitation at room temperature, the emission spectrum exhibits only the unresolved

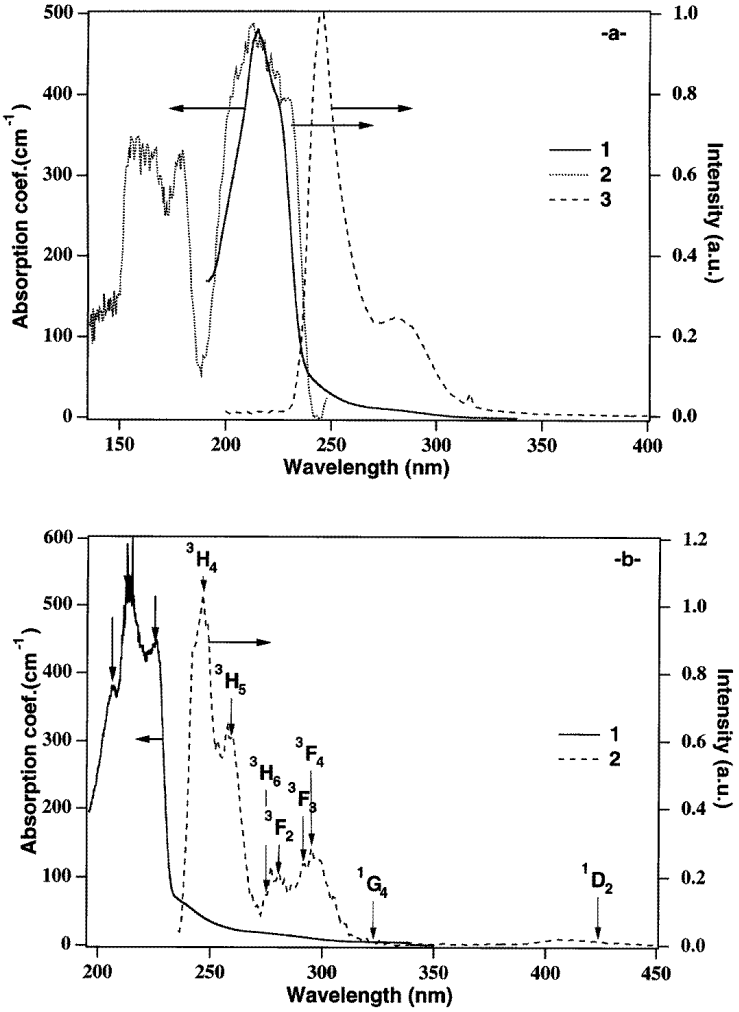


**Figure 2.** $LuAlO_3:Pr^{3+}$. (a) At room temperature. 1: the absorption spectrum; 2: the excitation spectrum ($\lambda_{em} = 260$ nm); and 3: x-ray-induced emission. (b) 1: the absorption spectrum at $T \approx 10$ K; and 2: the UV-induced emission at $T \approx 10$ K ($\lambda_{exc} = 230$ nm).

band of $Ce^{3+}$ ions.

We should point out that no garnet phases are present in our crystals, since we did not observe the green emission that Moses *et al* [9] saw. This is in good agreement with our x-ray diffraction measurements.

The emission band appearing in the region 250–320 nm under x-ray excitation cannot be related to the $Ce^{3+}$ fluorescence, since it occurs in the range of the $Ce^{3+}$ absorption. This emission had already been observed, and assigned to self-trapped excitation [12].

The optical properties of $LuAlO_3:Pr^{3+}$ are presented in figure 2. The fundamental electronic configuration of $Pr^{3+}$ is $4f^2$, with many excited states, and $^3H_4$ as the ground state. The absorption spectrum at liquid helium temperature exhibits three main absorption bands in the near-UV region (figure 2(b)), peaking at 206 nm, 214 nm, and 225.6 nm. These bands are assigned to the $4f^2(^3H_4) \rightarrow 4f5d$ transitions. Similarly to the case for

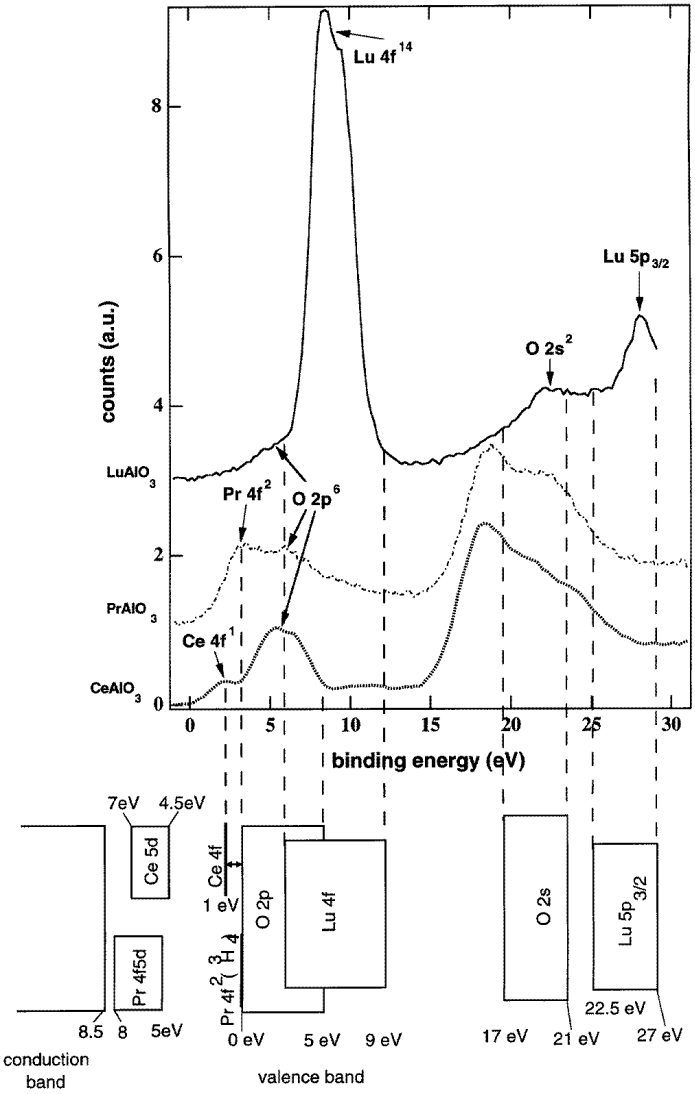


**Figure 3.** XPS spectra of $LuAlO_3$, $CeAlO_3$, and $PrAlO_3$. The energy level scheme is deduced from the XPS and excitation spectra of $LuAlO_3$:$Ce^{3+}$ and $LuAlO_3$:$Pr^{3+}$.

$Ce^{3+}$, the 5d levels of $Pr^{3+}$ split into two groups of $t_2$ and e levels. The e levels can be detected through the excitation spectrum at wavelengths below 200 nm (figure 2(a)). The peak at 179 nm is assigned to the absorption of one of the two e levels, while the other one at lower wavelengths is not clearly identified, because of the overlap with the band-to-band transition. The maximum of the absorption coefficient is around 600 $cm^{-1}$, ten times that of $LuAlO_3$:0.05 at.% Ce. If we consider that the oscillator strengths of f $\rightarrow$ d transitions are roughly the same for $Ce^{3+}$ and $Pr^{3+}$ ions, we can deduce that the real Pr concentration in $LuAlO_3$ is much higher than 0.05%.

The long tail observed probably has the same origin as the 250 nm absorption observed in $LuAlO_3$:$Ce^{3+}$, since the crystal also exhibits a 650 nm fluorescence when a 250 nm

excitation is used [20].

The emission spectra taken under x-ray synchrotron and laser excitations at room and low temperatures are shown in figures 2(a) and 2(b). Under 230 nm laser excitation, the spectrum exhibits at $T = 10$ K several bands which reflect the transitions from the lowest 5d state to the different states of the $4f^2$ configuration. In figure 2(b) are reported the calculated energies of the excited states related to $^3H_4$ for $LaF_3$:$Pr^{3+}$, supposing that the band of highest energy is assigned to the 4f5d $\rightarrow$ $^3H_4$ transition [18]. A very good agreement with experimental data can be seen.

The weak peak observed at 316 nm (figures 2(a)) is attributed to $Gd^{3+}$ impurities, as in the Ce-doped compound.

### *3.2. X-ray photoelectron spectra*

In order to understand the type and the energy of the electronic excitations formed at various energy excitations larger than the bandgap energy of the crystal, it is very important to have a knowledge of the band structure of the crystal and of the impurity-ion energy level positions. The technique of electron spectroscopy can be used to obtain the energies of the core levels in the crystal. X-ray photoelectron spectroscopy (XPS) measurements were performed on various scintillating materials [21], and the results for compounds with the perovskite-like structure were used to construct the energy level schemes presented in figure 3. These measurements give information about the energies of the levels, taking as a reference the Fermi level of the crystal. In our schemes, we have chosen arbitrarily as the origin of the energy the top of the valence band. On the basis of XPS measurements on $LuAlO_3$, we have represented the valence band formed by the 2p levels of $O^{2-}$, the 4f levels ($4f_{7/2}$ and $4f_{5/2}$) of $Lu^{3+}$ which overlap the valence band, the 2s levels of $O^{2-}$, and the 5p levels ($5p_{3/2}$ and $5p_{1/2}$) of $Lu^{3+}$. The low concentration of $Ce^{3+}$ or $Pr^{3+}$ ions prevents us from obtaining direct information about the position of the 4f levels of the dopants from the XPS technique. We have therefore performed measurements on $CeAlO_3$ crystal fibres grown in our laboratory, and $PrAlO_3$ powders. The 4f level of $Ce^{3+}$ was found to lie 1 eV above the top of the valence band. The $4f^2$ level of $Pr^{3+}$ is at the same energy as the top of the valence band. We observed the same situation for $CeF_3$ and $PrF_3$. In the fluoride crystals the energy difference between the 4f level and the top of the valence band is smaller for $Pr^{3+}$ ions (3.1 eV) than for $Ce^{3+}$ ions (4.7 eV) [21]. Using these data, we estimate that in $LuAlO_3$ crystals the 4f level of Ce lies 1 eV above the top of the valence band, and the 4f level of Pr overlaps the valence band.

We had to estimate the forbidden bandwidth of $LuAlO_3$. The bandgap of $YAlO_3$ was calculated as around 8 eV [22, 23]. Excitation spectra obtained for the mixed powder $Lu_{1-x}Y_xAlO_3$:$Ce^{3+}$ exhibit a regular decrease of the band-to-band transition energy, as $x$ is increased from 0 to 1 [24]. The total shift from $LuAlO_3$ to $YAlO_3$ is 0.5 eV, leading to a forbidden bandwidth of 8.5 eV for $LuAlO_3$. The bottom of the conduction band is composed of the 5d levels of $Lu^{3+}$, and 3s and 3p levels of $Al^{3+}$. Finally, from UV absorption measurements, it is easy to see that the excited states of $Ce^{3+}$ and $Pr^{3+}$ ions are located in the bandgap of the crystal (figure 3).

### *3.3. VUV absorption*

The absorption spectrum from 7 to 50 eV (figure 4(b)) has been calculated from the reflectivity measurement using the Kramers–Krönig transformations. In this energy range, the absorption is only due to the host crystal, and the structure of the spectrum is the same

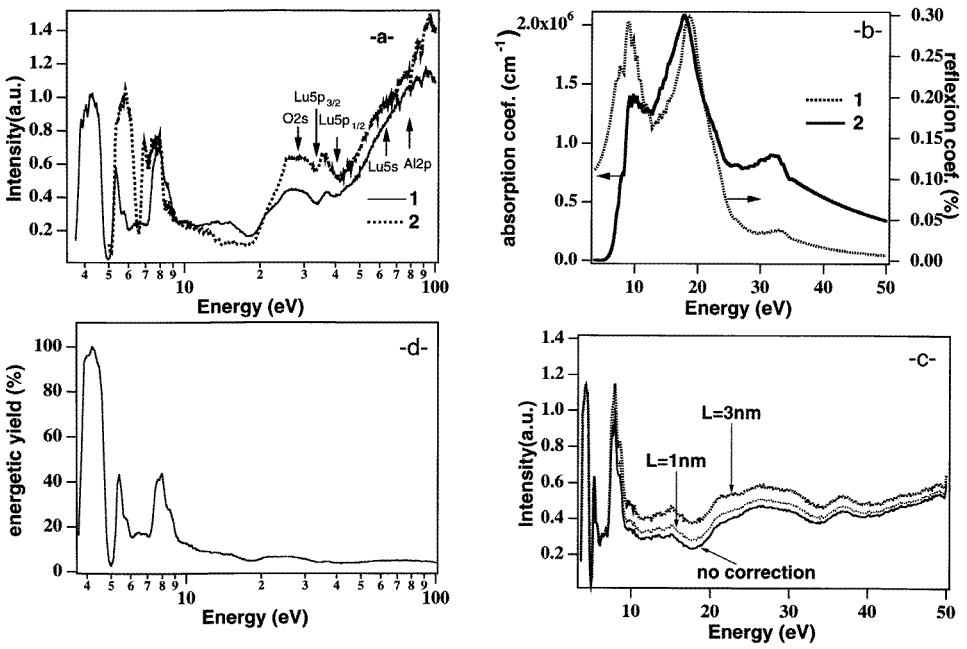


**Figure 4.** (a) 1: $LuAlO_3$:$Ce^{3+}$; the excitation spectrum ($\lambda_{em} = 360$ nm) from 3.5 to 100 eV; and 2: $LuAlO_3$:$Pr^{3+}$; the excitation spectrum ($\lambda_{em} = 260$ nm) from 5 to 100 eV. The arrows show the energy difference between the core levels and the bottom of the conduction band. (b) $LuAlO_3$: 1: the reflectivity; and 2: the absorption calculated from the reflectivity. (c) $LuAlO_3$:$Ce^{3+}$: the excitation spectrum corrected from the reflectivity, and the surface loss effect for different excitation diffusion lengths. (d) $LuAlO_3$:$Ce^{3+}$; the energetic yield (curve 2 in (a) divided by the excitation energy).

for both Ce-doped and Pr-doped systems. The absorption in the region 7.5 eV–12 eV is attributed to the transition from 2p($O^{2-}$) states to the bottom of the conduction band. In this region, the absorption spectrum of $LuAlO_3$ is similar to the absorption spectra of the $YAlO_3$ crystal taken for different polarizations of the incident light and at different temperatures [25]. But the $LuAlO_3$ absorption spectrum is very different from those generally observed for alkali halide crystals, which exhibit a strong excitonic peak at energies slightly lower than those of the band-to-band transitions. Nevertheless, the small hump observed at 8.1 eV for $YAlO_3$ [25] and at 8.3 eV for $LuAlO_3$ can be assigned to exciton formation. The relative intensities of the peaks due to inter-band transitions and to excitons show that the direct creation of electron–hole pairs is more probable than direct exciton formation.

The strong absorption band of triangular shape from 12 eV to 24 eV with a maximum near 18 eV is attributed to 4f($Lu^{3+}$) $\rightarrow$ 5d($Lu^{3+}$) allowed transitions, and its width is the sum of the 4f($Lu^{3+}$) and 5d($Lu^{3+}$) bandwidths. These wide-band transitions originate from the oxygen valence band, which starts at 8.5 eV. According to the XPS results of figure 3, the structures observed at 26 eV and 32 eV can be assigned to transitions from the 2s($O^{2-}$) and $5p_{3/2}$($Lu^{3+}$) levels to the conduction band. The absorption of the $5p_{1/2}$($Lu^{3+}$) level has not been observed, since the intensity of the reflectivity above 35 eV is too weak, due to the exhaustion of the electronic transitions. The shape of the absorption spectrum above this energy is the result of an extrapolation of the reflectivity using an $\omega^{-4}$-dependence, because integrals over domains extending to infinity are needed for Kramers–Krönig calculations.

### *3.4. Luminescence excitation spectra in the VUV*

For UV excitation energy, the absorption coefficient is very high, due to the host crystal absorption. The energy transfer to the dopant can be studied in this region.

For excitation energies higher than the energy of the 4f $\rightarrow$ 5d ($Ce^{3+}$) transitions, the excitation spectrum of $LuAlO_3$:$Ce^{3+}$ exhibits a weak broad band at 6.3 eV. Such structure has been observed in several crystals doped with $Ce^{3+}$ [26]. It has been attributed to a self-trapped exciton formed as the result of ionization of cerium, with the hole remaining on the $Ce^{3+}$. In some alkaline-earth fluorides doped with $Eu^{2+}$ or $Yb^{2+}$ ions, such a process is well established [27, 28]. In cerium-doped crystals, the confirmation of this process will have to be provided by further experiments; the band may be due to a 4f $\rightarrow$ 6s forbidden transition, which can be partially allowed by the mixing of the 6s states with conduction band states.

Since the onset of the fundamental absorption of $LuAlO_3$ occurs at around 7 eV, it is reasonable to attribute the increase of the light yield observed in figure 4(a) at 7.4 eV to the transfer from electron–hole pairs or excitons to $Ce^{3+}$. In the case of $LuAlO_3$:$Pr^{3+}$, this absorption overlaps the 4f $\rightarrow$ 5d transition.

From the excitation spectra measured between 4 and 100 eV (figure 4(a)), the light yield decreases after the fundamental absorption of $LuAlO_3$ has occurred, and reaches its initial value (obtained by direct excitation of $Ce^{3+}$) at 60 eV excitation energy. Nevertheless, the initial part of the excitation spectrum is perturbed by the strong reflection coefficient ($R \approx 30\%$) and absorption coefficient ($\approx 2 \times 10^6$ cm$^{-1}$) (figure 4(b)). In the region from 9 to 30 eV, there is an anticorrelation between the excitation and absorption. Such anticorrelation can be explained by surface losses. When $\alpha d \gg 1$ ($\alpha$ is the absorption coefficient, and $d$ is the thickness of the sample ($\approx$1 mm), it was shown [29, 30] that the measured light yield $\eta(h\nu)$ may be related to the volume light yield $\eta_0(h\nu)$ according to the relation

$$\eta(h\nu) = \frac{\eta_0(h\nu)}{1 + \alpha(h\nu)L}(1 - R)$$

where $L$ is the diffusion length of the electronic excitations. The result after correction for surface losses is presented in figure 4(c). For $L$-values between 1 and 3 nm, the correction does not change the excitation shape, from 10 to 50 eV. We consider then that the structures observed are mainly due to changes of energy transfer instead of surface loss effects.

Since the dopant concentration is low, excitation by impact has a low probability. The first multiplication edge in $LuAlO_3$ is expected to be at an energy higher than twice the gap of the host ($2E_g \approx 17$ eV). The increase of the light yield in this region could then be assigned to the increase of the number of the secondary excitations. As the full width of the valence band (O 2p + Lu 4f) is around 10 eV (figure 3), all of the photons with energies larger than 27 eV lead to secondary excitations. Some of such photons are already able to create three secondary excitations when they come from the top of the valence band, and an increase of the light yield can be expected. But instead of an increase, the spectrum exhibits a plateau (figure 4(a)). This is in agreement with the modelling of the luminescence excitation spectrum in the region of electronic excitation multiplication [31], which indicates that the second multiplication edge does not appear in wide-valence-band crystals ($E_v \approx E_g$).

Photons with energies above 26 eV are able to excite O 2s and Lu 5p core levels directly (figure 3). In figure 4(a) the photoionization threshold energies of the highest-lying core levels (energy differences between the core level and the bottom of the conduction band) are indicated. The number of secondary excitations can actually be reduced when the core levels are excited, since a deep hole is generated, instead of the creation of a

**Table 1.** Results of the fitting of the kinetics for $LuAlO_3$:0.05 at.% $Ce^{3+}$ and $LuAlO_3$:$Pr^{3+}$ obtained with different excitation energies at room temperature.

| $LuAlO_3$:0.05 at.% $Ce^{3+}$ | | | | $LuAlO_3$:$Pr^{3+}$ | | | |
|---|---|---|---|---|---|---|---|
| Energy (eV) | Decay time (ns) | Rise time (ns) | % slow component | Energy (eV) | Decay time 1 (ns) | Decay time 2 (ns) | % slow component |
| 4 | 17.1 | < 0.5 | | | | | |
| 5.16 | 17.5 | < 0.5 | 4 | 5.6 | 7.8 | | 9 |
| 6.5 | 17.9 | < 0.5 | 4 | 7.3 | 7.8 | | 21.4 |
| 8 | 17.4 | 2.3 | 18.5 | 8 | 7.7 | | 18.5 |
| 8.55 | 22.4 | < 0.5 | 35 | 16 | 9.3 | | 17 |
| 10 | 23 | 0.8 | 35 | 20 | 8.7 | | 15 |
| 16 | 21.4 | 0.9 | 25 | 25 | 8.2 | 20.7 | 12 |
| 20 | 21.6 | 0.9 | 29 | 28 | 8.2 | 19 | 12.4 |
| 25 | 21.6 | 0.9 | 31 | 33 | 6.9 | 13.9 | 11.6 |
| 28 | 21.6 | 0.9 | 28 | 35 | 7.3 | 15.6 | 12.8 |
| 35 | 21.4 | 0.8 | 29 | | | | |

hot electron occurring. For example, a 29 eV photon can produce different numbers of electronic excitations, according to whether the excited electron originates from the middle of the O 2p or the middle of the O 2s band. In the former case, the electron generated has a kinetic energy of 18 eV, which allows the generation of two secondary excitations. In the latter case, the kinetic energy of the electron is only 1.5 eV, which cannot lead to the multiplication of the excitations. The Auger relaxation of the O 2s core hole can excite an electron from the middle of the O 2p band to the conduction band, with a kinetic energy of 8 eV, with no possibility of the multiplication of excitations. Summarizing, the same 29 eV photon can create directly either an O 2p hole with the production of two secondary excitations, or an O 2s hole with the production of one secondary excitation. The efficiency of the latter process is of course at its maximum when the incident photon energy is resonant with the ionization energy of the core level.

Above 45 eV excitation energy, both excitation spectra exhibit an increase of the fluorescence intensity. The energetic yield of $LuAlO_3$:$Ce^{3+}$ ($\eta_0(h\nu)/E_{exc}$) is presented in figure 4(d). It is almost stable above 40 eV. After normalization of the 4f $\rightarrow$ 5d band, the energetic yield is measured as being 5–6%. The energy of the emitted photons (360 nm) is $\approx$3.4 eV. Under $\gamma$-excitation, it is therefore expected to be around 14 500–17 500 photons $MeV^{-1}$, in good agreement with the values obtained with small $LuAlO_3$:$Ce^{3+}$ samples from direct measurement of the light yield, using a $\gamma$-ray source [7]. This means that the energy-transfer mechanism for excitation energy above the first multiplication edge does not change.

### *3.5. Luminescence kinetics*

Some typical fluorescence decays of $LuAlO_3$:$Ce^{3+}$ are presented in figure 5. From the analysis of the decay profiles, we extracted three values: the rise time, the fall time, and the fraction of the slow component. The latter is the ratio of the background signal to the total number of counts. The rise and fall times are given by the fit of the data, taking into account the impulse response of the experimental set-up. The kinetics parameters are gathered together in table 1.

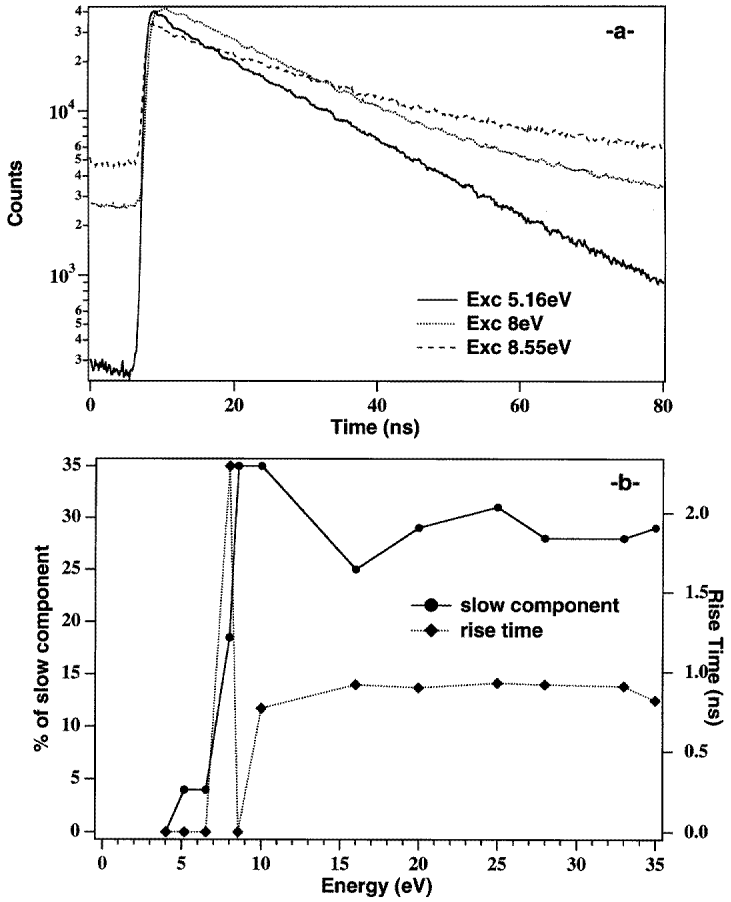


**Figure 5.** $LuAlO_3:Ce^{3+}$. (a) The kinetics for three excitation energies (5.16 eV, 8 eV, and 8.55 eV). (b) The slow-component fraction and rise time observed in the kinetics for different excitation energies.

The fluorescence decays are exponential for excitation energy below 8 eV. For these excitation energies, in addition, a transient appears with a rise time of around two nanoseconds, depending upon the Ce concentration. For higher energies up to x-ray ones, the transient still occurs, with a shorter rise time of less than one nanosecond.

In figure 5 are plotted the slow-component fraction, and the rise-time dependence on the energy excitation for the Ce-doped material. The Ce compound exhibits a small fraction of the slow component without a rise time, for the excitation energies of 5 and 6.5 eV. These energies correspond to $4f \rightarrow 5d$ transitions of $Ce^{3+}$. Below 5 eV excitation, the states involving the 5d level lie 2.5 eV below the bottom of the conduction band. The ionization process would involve many phonons, and thus has a low probability. Such excitation can be absorbed by traps, and then transferred to $Ce^{3+}$, resulting in a delay of the cerium emission. The traps are probably related to defects, which induce the 250 nm absorption (5 eV $\approx$ 248 nm). A study is in progress in order to confirm the correlation between the slow component of the $Ce^{3+}$ fluorescence decay and the 250 nm absorption. The same behaviour is observed for $LuAlO_3:Pr^{3+}$ (excitations at 5.16 and 6.5 eV).

## 4. Discussion

This section is devoted to the description of a possible energy transfer to the activator. The cerium ion can be excited directly or through two main processes: radiative or non-radiative energy transfer from excitons, and sequential hole and electron captures involving a charge transfer. It should be noted that the probability of the excitation of activators through the Auger process is very low in lightly doped systems, and, in addition, the Ce 5p–Ce 4f Auger transition is forbidden even for $CeF_3$ [31]. Both energy- and charge-transfer mechanisms lead to differences in the excitation spectra, for which a modelling is presented in figure 6, from reference [32]. For energy just above $E_g$, the light yield is expected to decrease in the case of energy transfer, and to increase in the case of charge transfer. This is explained by the decrease of the number of geminate electron–hole pairs when the excitation energy increases. At higher energy, the shape of the excitation spectrum is controlled by the multiplication of the secondary excitations, which depends upon the valence bandwidth.

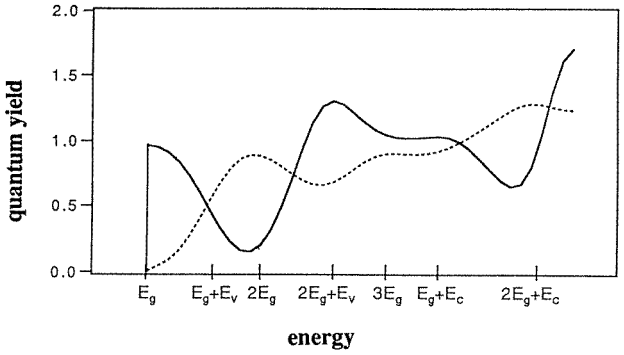


**Figure 6.** Quantum yields of the two recombination channels: the solid line is for excitons, while the dashed line is for separated electron–hole pairs. These curves are reproduced from reference [32].

At the fundamental absorption edge of $LuAlO_3$, the excitation spectrum exhibits a maximum of intensity comparable with the intensity observed for direct 4f–5d excitation of $Ce^{3+}$ (figure 4(a)) (or $Pr^{3+}$, figure 4(a)). Since, at 8 eV, the absorption coefficient is 2–3 orders of magnitude higher, absorption of $Ce^{3+}$ ($Pr^{3+}$) can be neglected. 8 eV excitation leads to close electron–hole pairs or excitons. The absorption spectrum shows that the dominant process is the creation of pairs of strongly correlated electrons and holes. These pairs can be considered as free excitons. They are able to migrate along a long distance, and then to transfer their energy to the $Ce^{3+}$ ($Pr^{3+}$) ions. From the shape of the excitation spectrum, we can conclude that excitonic transfer to $Ce^{3+}$ is very efficient in this excitation energy region.

The capture of the hole by $Ce^{3+}$ and $Pr^{3+}$ is favourable, since cerium and praseodymium are stable in the tetravalent state. The probability of this process strongly depends upon the energy difference between the top of the valence band, and the ground level of the activator. We saw previously that this energy separation is 1 eV for crystals doped with $Ce^{3+}$ (0 eV for the crystal doped with $Pr^{3+}$). In fact, this energy mismatch is less than 1 eV if the relaxation of the host lattice is taken into account, resulting in a shift of the configuration curves of the $Ce^{3+} + e_c + h_v$ and $Ce^{4+} + e_c$ states after the hole capture by $Ce^{3+}$ [12]. If

the lifetime of the localized hole on the ion is longer than the electron trapping time, a slow component appears in the fluorescence decays of lightly doped crystals [29].

Table 1 shows that the fluorescence decay time changes at 8.5 eV excitation energy. For excitation energies below 8.5 eV, it is ≈17.4 ns for $LuAlO_3:Ce^{3+}$ (≈7.8 ns for $LuAlO_3:Pr^{3+}$). For these excitation energies, the dopant is excited directly or through exciton transfer. Above 8.5 eV excitation energy, the fluorescence decay time is above 21 ns for $Ce^{3+}$ (above 8 ns for $Pr^{3+}$). We suppose then that the differences in the kinetics are due to the change of the transfer mechanism. Charge transfer to $Ce^{3+}$ or $Pr^{3+}$ involves first the capture of a valence band hole by the 4f state of the dopant, and then an electron trapping in the 5d state of $Ce^{3+}$. These two captures occur with a different timing. The electron trapping by the relaxed $Ce^{4+}$ ion is followed by the $Ce^{3+}$ relaxation in the excited states. The hole trapping by $Ce^{3+}$ or $Pr^{3+}$ can be delayed by the valence band hole autolocalization, which induces slower stepwise mobility, or by hole trapping by any other defects. Such delays change the kinetics of the fluorescence, inducing rise times and long components in the fluorescence decays. Further experiments using specific techniques (EPR, thermoluminescence, thermal conductivity, ...) are needed to describe the electronic structure of the defects, and then to establish the origin of delays, by modelling the decays using the kinetic equation involving the trap parameters deduced experimentally, as was done previously for $Lu_2SiO_5:Ce^{3+}$ [33].

The analysis of the region of the excitation spectrum where one of the two energy-transfer mechanisms dominates shows that the energy transfer from an exciton is more efficient than the transfer through the sequential capture of the hole and the electron by $Ce^{3+}$ or $Pr^{3+}$. The absence of excitonic transfer for excitation energies larger than 8 eV can be understood by considering the low probability of exciton formation by hot electrons. Indeed, this probability is determined by the energy-loss function, which is itself related to the absorption. In the region around 8 eV, the spectrum does not exhibit a strong excitonic peak (figure 4(b)). The $Pr^{3+}$-doped crystal exhibits the same behaviour as regards the energy-transfer mechanism.

## 5. Concluding remarks

The results obtained show that the energy transfer of the electronic excitations induced by a high-energy photon absorption to fluorescent dopant ions occurs mainly through a sequential electron–hole trapping process. The probability of forming excitons with hot electrons is actually low for $LuAlO_3$.

The $Pr^{3+}$-doped crystals exhibit the same mechanism of transfer. It should be even more efficient than that for $LuAlO_3:Ce^{3+}$, since the $Pr^{3+}$ 4f level lies near the top of the valence band. Unfortunately, under $\gamma$-ray excitation, $LuAlO_3:Pr^{3+}$ does not exhibit any photopeak, whereas $LuAlO_3:Ce^{3+}$ gives rise to a well-resolved photopeak [34]. The broadening of the photopeak is substantial in the latter system, reflecting not only inhomogeneities, but also the reabsorption of the fluorescence in the crystal due to the overlap between the emission and the absorption bands. In the case of the praseodymium-doped crystal, this overlap is particularly large, which could explain the absence of the photopeak.

The development of $LuAlO_3$-doped scintillators requires the study of hole localization, as well as the electronic structures of the traps. These localized levels have a strong influence on the transfer mechanisms, but also they can induce parasitic absorption, which limits the light yield in the case of large crystals.

**Acknowledgments**

This work was partially supported by two programmes of the European Economic Community: 'Human Capital and Mobility', contract number CHRX-CT93-0108, and the INTAS Program, contract number INTAS-93-2554, and also by the NATO grant ATECH.CRG 940392. It was performed within the framework of the 'Crystal Clear' Collaboration, CERN Research and Development project RD-18.

**References**

[1] van Eijk C W E 1994 *Proc. Int. Workshop PHYSCI '94 on Physical Processes in Fast Scintillators (St Petersburg, 1994)* p 1
[2] Mikhailin V V 1995 *Nucl. Instrum. Methods Phys. Res.* B **97** 530
[3] Pedrini C, Bouttet D, Dujardin C, Moine B, Dafinei I, Lecoq P, Koselja M and Blazek K 1994 *Opt. Mater.* **3** 81
[4] Korzhik M V, Misevish O V and Fyodorov A A 1992 *Nucl. Instrum. Methods* B **72** 499
[5] Mares J A, Nikl M, Pedrini C, Moine B and Blazek K 1992 *Mater. Chem. Phys.* **32** 342
[6] Suzuki H, Tonbrello T A, Melcher C L and Schweitzer J S 1992 *Nucl. Instrum. Methods* A **320** 263
[7] Lempicki A, Berman E, Wojtowicz A J, Balcerayk M and Boatner L A 1993 *IEEE Trans. Nucl. Sci.* **40** 384
[8] Melcher C L and Schweitzer J S 1992 *Nucl. Instrum. Methods* A **314** 212
[9] Moses W W, Derenzo S E, Fyodorov A, Korzhik M, Getkin A, Minkov B and Aslanov V 1995 *IEEE Trans. Nucl. Sci.* **42** 275
[10] Lempicki A, Randles M H, Wisniewski D, Balcerzyk M, Brecher C and Wojtowicz A J 1995 *IEEE Trans. Nucl. Sci.* **42** 280
[11] Dujardin C, Pedrini C, Bouttet D, Verweij J W M, Petrosyan A G, Belsky A N, Vasil'ev A N, Zinin E I and Martin P 1996 *Proc. Int. Conf. on Inorganic Scintillators and Their Applications, SCINT '95* (The Netherlands: Delft University Press) pp 336–9
[12] Wojtowicz A J 1996 *Proc. Int. Conf. on Inorganic Scintillators and Their Applications, SCINT '95* (The Netherlands: Delft University Press) pp 95–102
[13] Lempicki A, Brecher C, Wisniewski D and Zych E 1996 *Proc. Int. Conf. on Inorganic Scintillators and Their Applications, SCINT '95* (The Netherlands: Delft University Press) pp 340–3
[14] Petrosyan A G 1994 *J. Cryst. Growth* **139** 372
[15] Petrosyan A G and Pedrini C 1996 *Proc. Int. Conf. on Inorganic Scintillators and Their Applications, SCINT '95* (The Netherlands: Delft University Press) pp 498–501
[16] Belsky A N, Vasil'ev A N, Mikhailin V V, Gektin A V, Shiran N V, Rogalev A L and Zinin E I 1992 *Rev. Sci. Instrum.* **63** 806
[17] Weber M J 1973 *J. Appl. Phys.* **44** 3205
[18] Dieke G H 1968 *Spectra and Energy Levels of Rare Earth Ions* ed H M Crosswhite (New York: Interscience)
[19] Gumanskaya E G, Egorcheva O A, Korzhik M V, Smirnova S S, Povlenko V B and Fedorov A A 1992 *Opt. Spectrosc.* **72** 215
[20] Dujardin C, Pedrini C, Meunier-Beillard P, Moine B, Gâcon J C and Petrosyan A 1997 *Int. Conf. on Luminescence and Optical Spectroscopy of Condensed Matter (Prague, 1996); J. Lumin.* at press
[21] Bouttet D, Dujardin C, Pedrini C, Brunat W, D Tran Minh Duc and Gesland J Y 1996 *Proc. Int. Conf. on Inorganic Scintillators and Their Applications, SCINT '95* (The Netherlands: Delft University Press) pp 111–3
[22] Tomiki T, Fukudome F, Kaminao M, Fujisawa M and Tanahara Y 1986 *J. Phys. Soc. Japan* **55** 2090
[23] Tomiki T, Fukudome F, Kaminao M, Fujisawa M, Tanahara Y and Futemna T 1988 *J. Lumin.* **40+41** 379
[24] Meunier-Beillard P *et al* 1997 *Int. Conf. on Luminescence and Optical Spectroscopy of Condensed Matter (Prague, 1996);* unpublished results
[25] Tomiki T, Kaminao M, Tanahara Y, Futemna T, Fujisawa M and Fukudome F 1991 *J. Phys. Soc. Japan* **5** 1799
[26] Mayolet A 1995 *PhD Thesis* Université Paris XI
[27] Moine B, Pedrini C and Courtois B 1991 *J. Lumin.* **50** 31
[28] Dujardin C, Moine B and Pedrini C 1993 *J. Lumin.* **54** 259
[29] Pedrini C, Belsky A N, Vasil'ev A N, Bouttet D, Dujardin C, Moine B, Martin P and Weber M J 1994 *Materials Research Society Symposium Proceedings* vol 348 (Philadelphia, PA: Materials Research Society)

pp 225–34
[30] Pedrini C, Bouttet D, Dujardin C, Belsky A and Vasil'ev A 1996 *Proc. Int. Conf. on Inorganic Scintillators and Their Applications, SCINT '95* (The Netherlands: Delft University Press) pp 103–10
[31] Vasil'ev A N 1996 *Nucl. Instrum. Methods Phys. Res.* B **107** 165
[32] Kamenskikh I A, Mikhailin V V, Shpinkov I N and Vasil'ev A N 1989 *Nucl. Instrum. Methods Phys. Res.* A **282** 599
[33] Kamenskikh I A, Mikhailin V V, Petrovykh D Y, Vasil'ev A N, Munro I H, Mythen C, Shaw D A, Becker J, Schroeder A, Zimmerer G and Makhov V N 1996 *Proc. Int. Conf. on Inorganic Scintillators and Their Applications, SCINT '95 (Delft)* abstracts, p 129
[34] Moszynski M, Dowolski, Ludziejewski T, Lempicki A, Brecher C, Wisniewski and D and Wojtowicz A J 1996 *Proc. Int. Conf. on Inorganic Scintillators and Their Applications, SCINT '95* (The Netherlands: Delft University Press) pp 348–51